Effect of block length on the network connectivity and temperature resistance of model, soft thermoplastic elastomers

Simone Sbrescia[1], Paola Nicolella[2], Tom Engels[3], Michelle Seitz[3]

1) Bio and Soft Matter Division (BSMA), Institute of Condensed Matter and Nanosciences (IMCN), Université Catholique de Louvain, Louvain-la-Neuve, Belgium.
2) Department of Chemistry, Johannes Gutenberg-Universität Mainz, Duesbergweg 10-14, Mainz D-55128, Germany.
3) Materials Science Center, DSM, Geleen, The Netherlands.

Abstract

We discuss the connection between high-temperature mechanics, block structure, and composition of a model series of industrially relevant, soft, thermoplastic elastomers (TPEs) containing polydisperse hard blocks (HBs). The high-strain deformation behavior of these materials results from the combination of multiple dynamics in the system, i.e., the HB associations and the mobile and entangled amorphous phase. Many soft TPEs show a reduction in toughness with increasing temperature. Molecular weight (Mw) has been shown to improve the temperature-dependent mechanics by increasing network connectivity. In this work, we investigate the possibility to increase the network connectivity by tuning block length at constant Mw and composition. The average number of HBs per chain can be used to quantify network connectivity; however, by using block statistics, we show how increasing this value is not enough to increase the high-temperature mechanics, especially in the case of polydisperse HBs. Since temperature affects the HB ability to associate with each other, only the number of associated HBs per chain determines network connectivity. The experimental results are consistent with modeling predictions, revealing how decreasing the average block length influences the crystal stability, which ultimately controls network connectivity, and how this relationship is affected by temperature.

Introduction

Segmented block copolymers are a class of thermoplastic elastomers (TPEs) that combine the elasticity of thermoset rubbers with the melt processability and recyclability of thermoplastics. Their elasticity is due to physical associations which act as reversible crosslinks connecting a network of amorphous, mobile chains [1-9]. One advantage of TPEs is the possibility to easily tune their properties by modifying the relative amount of hard (HB) and soft blocks (SB) in the system or their respective block lengths. Polyether-ester systems with PTMO-based soft blocks and PBT hard blocks are common. These systems are commercially important with uses ranging from hot melt adhesives, breathable films, wire, and cable insulation, as well as fatigue-resistant ducts, boots, and bellows. This paper investigates how the HB length distribution determines the crystallinity and high strain mechanical response versus temperature for these commercially relevant TPEs.

One limitation of many soft-TPEs (HB wt% < 50%) is that they show a decrease in toughness and final extensibility as the temperature increases [10-14], opposite to what happens in many semicrystalline homopolymers. For temperatures higher than room temperature, the failure mechanism has been explained by modeling the material as a transient network in which failure occurs due to a loss of connectivity [12-14]. In brief, the physical associations between HBs are sensitive to stress, temperature, and time, as can be described by Eyring's flow theory [12, 15]. As the material is deformed, these associations gradually fail and the network chains are progressively disconnected from the percolated network ultimately leading to rupture. The interplaying network-connectivity and

disentanglement dynamics are responsible for the high-strain mechanics and failure behavior of these viscoelastic materials.

In this framework, the degree of connectivity is determined by the number of entanglements *and* the number of associated HBs per chain. Admittedly, network connectivity, and in general the mechanical properties, are also influenced by the microstructure achieved by the materials upon crystallization [2], i.e., by how the chains are linked together. The materials are obtained using the same processing conditions and show similarities in the linear properties at room temperature at fixed HB content. Hence, we can fairly assume that the initial microstructure is similar for samples with same HB amount. In this case, the governing and tunable parameter that influences network connectivity is the number of associated HBs per chain. Chains with more HBs per chain ($< N >$) can form better-connected structures allowing the material to withstand more dissociation events before chain pullout. Connectivity can be increased by increasing the molecular weight (Mw) of the chains at fixed composition (HB/SB ratio). This leads to higher temperature resistance [12-14, 16]. However, increasing Mw is often not industrially feasible due to the economics of long polymerization times or to processing limitations due to high melt viscosity. Alternatively, the number of HBs per chain can be increased by decreasing the HB length at fixed Mw and composition.

The effect of HB length on the morphology and the mechanical properties of block copolymers thermoplastic elastomers has been investigated at room temperature [4, 5, 9, 17, 18] but not at higher temperatures. Decreasing the HB length at fixed composition leads to an increase in blocks per chain but to a decrease in the melting temperature (T_m). However, our previous work [14] shows that the temperature resistance does not only scale with T_m. Thus, it is not obvious what the impact on mechanics at temperatures between room temperature and the melting point will be.

In this work, we investigate the effect of changing $< N >$ at fixed chain length on the thermomechanical properties for a series of model polyether-ester block copolymers. To increase $< N >$ at fixed Mw and SB/HB ratio, we use shorter SB. This leads to a decrease in HB length and consequently to a decrease in peak melting temperature T_m. However, we show that increasing $< N >$ in this way does not guarantee an increase in network connectivity, particularly at higher temperature. For systems with polydisperse hard blocks, not all the HBs are able to crystallize during cooling from the melt and thus to act as physical crosslinks. Gabrielse et al. [4] attributed the lower crystallinity of samples with on average shorter HBs to their having a higher fraction of HBs too short to be able to crystallize [19]. Due to entropic effects, decreasing the SB length leads to a lower degree of phase separation [20]. However, for these systems crystallization is the driving mechanism for phase separation [5, 21].

By accounting for block polydispersity, we show that the effective number of HBs per chain that crystallize does not increase with decreasing SB length. Depending on the testing temperature, the associated HBs per chain can even decrease with decreasing SB length despite the increase in nominal number of blocks, leading to poorer connected materials and lower temperature resistance. The outcomes show the nontriviality of the approach of simply considering the nominal number of HBs per chain as a measure for network connectivity, especially for samples with polydisperse HBs, where only a fraction of the HBs will crystallize on cooling from the melt. Using Flory's approach to model crystallinity versus temperature is useful to guide synthesis choices to tune resistance at higher temperatures.

Materials

Our model system is a poly(ether-ester) block copolymer based on polybutylene terephthalate (PBT) as HB, and poly(tetramethylene oxide) (PTMO) as SB obtained via transesterification followed by polycondensation of dimethyl terephthalate (DMT), 1,4-butanediol (BDO) and PTMO diol. Details on the synthesis procedure have been previously described [4]. After polymerization, the material is extruded and pelletized into granules.

Samples studied are summarized in Table I and have two different SB/HB ratios and SB lengths ($M_{n,SB}$) ranging from 1 kg/mol to 3 kg/mol. Materials are denoted by the wt% and length of PTMO used followed by the total number average molecular weight (M_n) of the block copolymer, e.g. 60_PTMO2k_29 is a polymer made with 60wt% of PTMO with $M_{n,SB}$ of 2 kg/mol and with total chain M_n of 29 kg/mol. The values for M_n are calculated from size exclusion chromatography as explained in our previous work [14]. Values related to the average sequence length of the HBs ($< Ln >$), e.g. the average number of PBT monomer units per HB, are listed in Table I.

Granules are compression molded into 200 µm thick sheets under vacuum at 230 ˚C and allowed to equilibrate for a few minutes at this temperature before being cooled to room temperature at a cooling rate of 20 ˚C/ min by cooling the press via an internal water circulation system. To define the thickness, Teflon sheets are used as molds, sandwiched between two more Teflon sheets to prevent sticking to the metal plates.

Table I – Composition and characteristics of polymers studied

Sample	SB_{wt}	$M_{n,SB}$[i]	$< Ln >$[ii]	$< N >$[iii]	x_{PBT}[iv]	E' at 23 °C[v]	E' at 100°C[v]	T_m peak[vi]	M_n
	[%]	[kg/mol]	[#]	[#]	[-]	[MPa]	[MPa]	[°C]	[kg/mol]
75_PTMO3k_32	75	3	4.96	6.65	0.8	20	9	180	32.3
75_PTMO2k_41	75	2	3.44	12.61	0.71	19	8	165	41.1
60_PTMO2k_29	60	2	6.47	8.07	0.84	47	25	200	29.4
60_PTMO1.4k_32	60	1.4	4.65	11.19	0.79	52	25	180	31.7
60_PTMO1k_30	60	1	3.43	14.39	0.71	41	19	165	29.7

[i] M_n of the PTMO diol

[ii] Average sequence length of the PBT segments

[iii] Average number of HBs per chain

[iv] PBT mole fraction

[v] Storage modulus obtained via DMTA

[vi] PBT melting peak maximum extracted from DSC

Methods

Differential Scanning Calorimetry (DSC)

DSC experiments are performed on a TA Instruments (USA) Q2000 instrument. Scans are performed at heating rates of 10 °C/min. Standard 40 µL aluminum pans are used and samples weighed ~3 mg. Tests are done in air and each pan is punctured prior the test to avoid any pressure build up. Samples are taken from the same films as for the mechanical tests.

Dynamic Mechanical Thermal Analysis (DMTA)

DMTA tests are performed on an RSA-3 TA Instrument (USA). Rectangular shaped samples (40 mm long, 2 mm wide) punched from the 200 µm hot-pressed films are tested in tension at heating rates of 5 °C/min and at a constant frequency of 1Hz in the temperature range from -120 °C to ~Tm in a nitrogen atmosphere.

Tensile tests

Tensile bars of ISO 527/5A standard shape are punched out of the 200 µm films and tested on a standard Zwick Roell (Germany) 1474 Universal tensile testing machine equipped with an air circulation oven. Engineering strain is determined using an optical extensometer for increased accuracy, especially in the high strain regime, where strain-hardening and some slippage from the grips are likely to occur. For all the tests at high temperatures, the samples are equilibrated at target temperature for 10 min before the test starts. During the tensile tests, samples are subsequently stretched at a constant crosshead speed until failure. A preload of 0.05 N (ca. 0.06 MPa) is applied before starting. The crosshead speed is set as 500 mm/min, corresponding to a strain rate, $\dot{\varepsilon}$, of 0.17 s^{-1}. The crosshead speed for the cyclic tests is set to 50 mm/min (0.017 s^{-1}). It must be noted that the crosshead speed is constant, hence the true strain rate is not. Deformation steps are indicated in the figures. As in the tensile test, a preload of 0.05 N is applied before starting. There is no holding time between cycles. Residual strains of each cycle i ($\varepsilon_{residual(i)}$) are collected corresponding to the values of strains where the force reached the preload value during unloading. Recovered strain is then calculated by subtracting the applied pre-strain ($\varepsilon_{applied(i)}$) and the residual strain of the respective i-th cycle. The tensile set (*TS*) is also calculated, and is defined as

$$TS = \frac{\Delta\varepsilon_{residual}}{\Delta\varepsilon_{cycle}}, \quad (1)$$

where,

$$\Delta\varepsilon_{residual} = \varepsilon_{residual(i)} - \varepsilon_{residual(i-1)} \quad (2)$$

and

$$\Delta\varepsilon_{cycle} = \varepsilon_{applied(i)} - \varepsilon_{residual(i-1)} \quad (3)$$

Wide Angle X-ray Scattering (WAXS)

The experiments are carried out on a GANESHA 300XL (SAXSLAB, USA) + system from JJ X-ray (Denmark). The instrument is equipped with a Pilatus 300 K (DECTRIS, Switzerland) detector, with a pixel size of 172 µm x 172 µm. The X-ray source is a Genix 3D (Xenoxs, France) Microfocus Sealed Tube X-Ray Cu-source with integrated Monochromator (multilayer optic “3D version” optimized for SAXS) (30 W). Calibration of scattering angle is done using silver behenate (d_001 = 58.380 Å). Multiple films of the same samples are stacked together to achieve ~1 mm thickness to improve the signal from WAXS. The stack is placed in an aluminum bag and in a Linkam temperature stage (UK). The heating

rate is set to 5 ˚C/min, and the WAXS acquisition time is 37 s, meaning that each measurement is averaged on a ΔT = 3 ˚C temperature range. The X-ray wavelength is 0.124 nm and the distance of the sample from the detector is 120 mm. The crystallinity index ($X_{x\text{-}ray}$) is calculated using PeakFit software from the ratio between the total area and the amorphous halo [22] in the q range from 0.5 to 2. The amorphous halo is fitted with a Pseudo-Voigt function.

Fourier Transform InfraRed (FTIR)

Spectra were collected with a Bruker Vertex 70 FT-IR Spectrometer (Germany) equipped with PIKE GladiATR heatable ATR (USA). The ATR crystal used was diamond. The resolution was 4 cm^{-1} and 200 scans per measurement were acquired with a scan speed 20kHz and collected with a MCT detector. The resulting spectra were analyzed with the Software Spectra Manager provided by JASCO®.

Previous works on pure PBT [23], PBT blends [23, 24] and PCL [24] show a gradual shifting of the absorption peak at ~1710 cm^{-1} (C=O stretching band) towards higher wave numbers as the crystals melt, up to ~1720 cm^{-1} when the material is completely amorphous. The same behavior is observed in our copolymers as well (Figure S1 supplementary materials). The peak can be seen as a superposition of crystalline and amorphous spectral components and the crystallinity can be calculated as the fraction of the crystalline part. Following He et al. [25], the peak has been deconvoluted into an amorphous (1720 cm^{-1}) and a crystalline peak (1710 cm^{-1}) with best fitting procedure. A custom crystallinity index has been then defined, X_{FTIR}, which accounts for the different HBwt% in the materials:

$$X_{FTIR} = \frac{Area\ 1710}{Area\ 1710 + Area\ 1720} \frac{HB_{wt\%}}{100} \quad (4)$$

Results and discussion

Block statistics calculation

The mechanical properties of block copolymers are strongly influenced by the number and length of their blocks, e.g., blocks too short are not able to crystallize. To start, we discuss the effect block statistics have on the crystallinity and connectivity of our systems over a wide temperature range using the models and analytical equations developed by Flory [19] and Frensdorff [26]. The goal is to provide a framework for understanding the high temperature thermomechanical response of our model systems.

Since every PTMO and BDO unit in the chain is always preceded and followed by a DMT, we can consider the system as made by only two main repeating units, i.e., PTMO-DMT and BDO-DMT (PBT monomer) as shown in Figure 1.

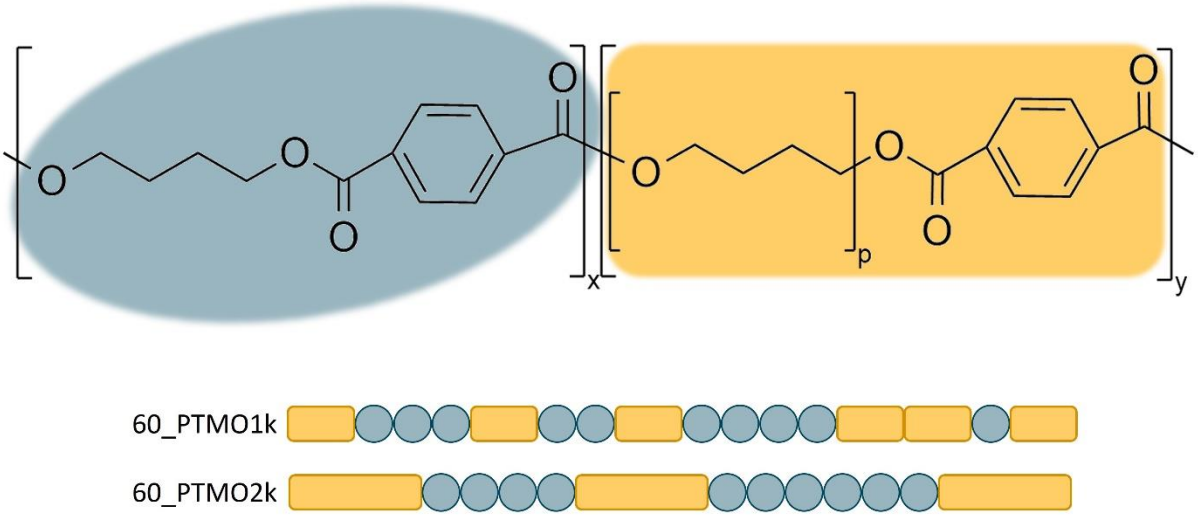

Figure 1 Chemical structure of the two repeating units used for the block statistics calculation. Schematic below illustrates possible chain structures for two polymers with differing SB length.

Assuming random copolymerization, the average length of the HB (expressed as the number of consecutive PBT monomer units) can be calculated following Deschamps [27]

$$< L_n > = 1/(1 - x_{PBT}) \quad (5)$$

where x_{PBT} is the mole fraction of PBT units. The number of HBs per chain, $< N >$,can be estimated with the approach of Frensdorff [26]

$$< N > = n * x_{PBT} * (1 - x_{PBT}) \quad (6)$$

with n being the average degree of polymerization of the total chain, here simply defined as:

$$n = M_n / \left[\frac{(M_{n,SB}) * SB_{wt\%}}{100} + \frac{(M_{0,PBT}) * HB_{wt\%}}{100}\right], \quad (7)$$

where $M_{0,PBT}$ = 220 g/mol.

Since blocks too short to crystallize do not contribute to the network connectivity, it can be useful to estimate the average number of HBs with length k or above ($< N_{L \geq k} >$), which can be calculated with an equation provided by Frensdorff [26] for copolymers with sequential monomer distribution governed by a given statistical law. In the case of random distribution, i.e., with a sequence propagation probability equal to x_{PBT}, the equation becomes:

$$< N_{L \geq k} > = n * (1 - x_{PBT}) * (x_{PBT})^k. \quad (8)$$

Figure 2 shows $< N_{L \geq k} >$ vs k estimated for our system. For systems with shorter SB, hence with shorter HBs on average, the number of nominal HBs per chain (e.g., k=1) increases. However, by only considering HBs that contain at least 3 PBT repeat units (k=3), there is close to no difference with varying SB length. For even longer HBs (e.g., k=4), using shorter SB actually reduces the number of long HB/chain.

In order to estimate the effective number of HBs per chain at a given testing temperature, $< N_{eff} >$, the next step is to link each temperature with a threshold value for the HB length (k^*) below which the HBs are too small to be stable in the crystalline form. Flory's theory of crystallization [19] has mostly been used to describe the shift in T_m with $< Ln >$ for these systems [28, 29]. However, in the same work, Flory also discusses the thermal stability of the crystalline blocks as a function of their

length. In his theory, only the equilibrium state is considered, ignoring transient effects resulting from crystallization kinetics. The case of random polydisperse blocks is also discussed, where HBs of different length have different thermal stabilities. Adopting the same model allows us to determine the values of $k^*(T)$ for which HBs of length $k < k^*(T)$ are not stable, while ones with length $k \geq k^*(T)$ can crystallize. Details about the derivation of $k^*(T)$ can be found in the supplementary materials.

Figure 3-a shows the trend of $k^*(T)$ with temperature, showing that at T<~150 ˚C all the curves are almost overlapping. At T>~150 ˚C, materials with shorter SB require longer HBs for crystal stability compared with systems with longer SB at the same T, to compensate for the lower driving force for crystallization given by a lower x_{PTB}. Figure 3-b shows $< N_{eff} >$ vs T, obtained by combining $k^*(T)$ with Equation 8, i.e., $< N_{eff} > = < N_{L \geq k^*(T)} >$. The results show a faster decrease of $< N_{eff} >$ for systems with shorter blocks as temperature increases. Since $< N_{eff} >$ is linked to network connectivity and temperature resistance, assuming that the crystals' structure and shape do not vary significantly between the materials, this model predicts that the materials with shorter blocks not only will not have a significant stronger temperature sensitivity, but also show lower temperature resistance at higher temperatures. To put it in another way, decreasing SB length at fixed total chain length is likely to only modestly increase connectivity at lower temperature and may even be detrimental to high temperature mechanical resistance.

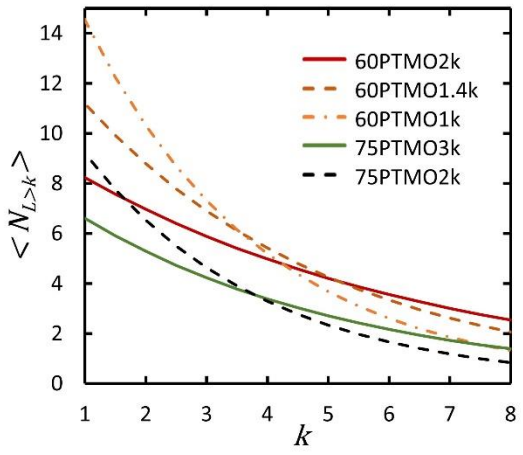

Figure 2 Average number of HBs per chain of at least k PBT repeat units estimated using Equation 8.

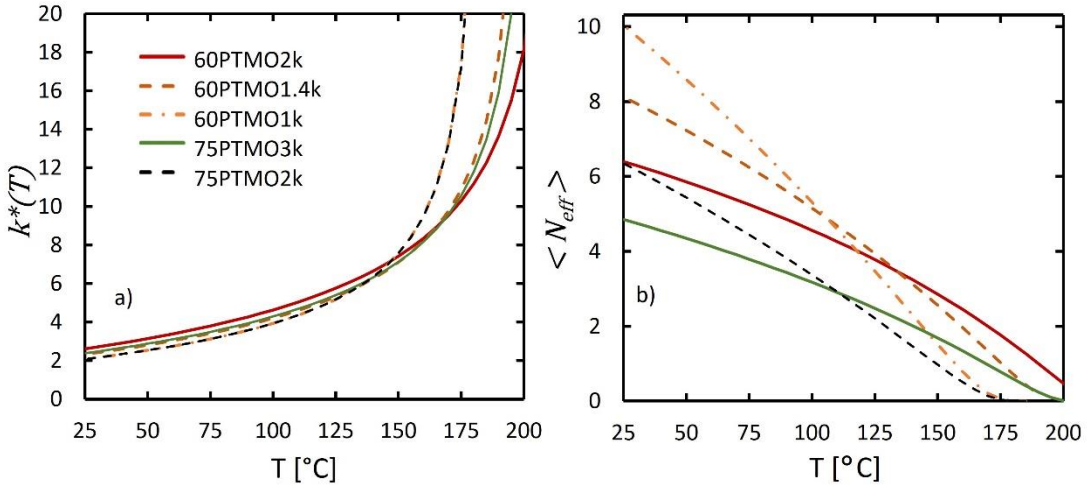

Figure 3 a) Minimum HB length below which crystals cannot form Vs temperature; b) Average number of HBs per chain long at least $k^*(T)$.

Under the strong assumption that the PBT sequences are not restricted in mobility by crystallization of other sequences in the same chain, another useful relationship has been developed by Flory [19] to describe the equilibrium crystallinity as a function of temperature as the sample cools down from the melt. Figure 4 shows the predicted crystallinity wt% vs temperature for the model systems. Since the PBT crystals act as physical crosslinks, ensuring network connectivity by preventing disentanglement of trapped entanglements, the trend of crystallinity vs temperature can be used to index the decrease of initial connectivity with increasing temperature.

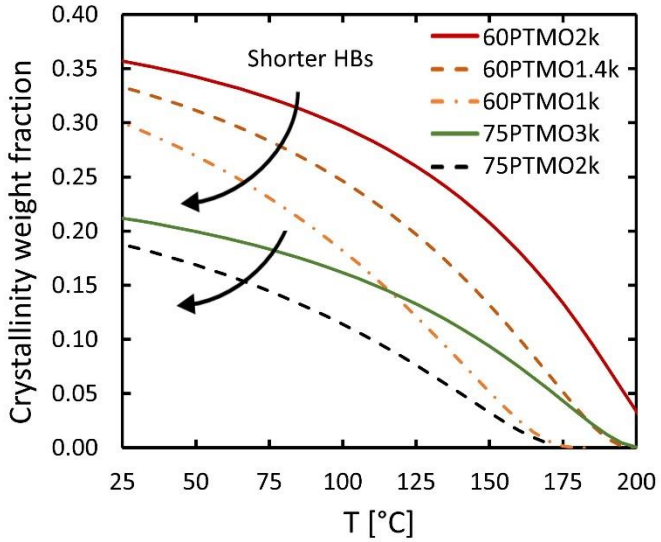

Figure 4 Crystallinity weight fraction within the TPE as a function of temperature as predicted by the Flory model.

Due to the assumption of the unrestricted mobility of the sequences of the same chains when crystallization occurs, and excluding any kinetics of crystallization, the values estimated from this model will be higher than those observed experimentally. Nonetheless, the qualitative behavior should be similar, and crystallinity decreases with temperature as a result of progressive melting of crystallites containing shorter HBs. Interestingly, the crystallinity decreases already at temperatures well below the peak melting temperatures. Additionally, it shows that the crystallinity decreases fastest with temperature for systems with shorter blocks on average consistent with the plots of Figure 3.

To summarize, combining the block statistics models from Flory and Frensdorff allows estimation of how $<N_{eff}>$ and crystallinity decrease with increasing temperature. The decrease occurs faster with decreasing SB length which suggests a faster decrease of network connectivity and high-temperature mechanical performances. In the next sections, we present the experimental results measuring crystallinity and mechanical properties with various techniques over a wide temperature range which show this is indeed the case.

Initial Morphology Characterization: *DSC, DMTA, X-ray, and FTIR*

Figure 5 shows DSC and DMTA results. Both the peak T_m of the PBT and PTMO crystals decrease to lower values as the SB length decreases. This is consistent with expectations from decreasing the HB

length and from previous work on similar samples [4, 9, 14]. It's worth emphasizing the broadness of the PBT melting peaks which is due to the HB length polydispersity. The T_m is indeed determined by the crystal thickness and perfection and increases with the average HB length ($< Ln >$) [4, 8]. The melting point of the PTMO SB and its relative crystallinity increases with SB length, consistent with previous results [30]. Cooling curves are shown in Supplemental Information.

All samples show qualitatively similar DMTA curves. From low to high temperatures, the samples show the melting of the PTMO crystals between ~-10 °C and 10 °C. Interestingly, PTMO crystallization is not detected in DSC or DMTA for the sample 60_PTMO1k_30, probably due to the difficulty of short PTMO segments to crystallize quiescently. At higher temperatures, a rubbery plateau is observed where E' slightly decreases with temperature until it drops faster as the temperature approaches T_m. In this region the elastic modulus is mainly determined by the PBT crystallinity [2, 14, 31]. The faster decrease in storage modulus (E') with temperature for the samples with shorter SB is consistent with the idea of more defected and less thick crystals generated in the samples with shorter SB. This also indicates that a significant degree of melting starts at temperatures much lower than the peak melting temperature for PBT from DSC, $T_{m,PBT}$. This is relevant since the degree of crystallinity at a given temperature is a strong indication of network connectivity and thus high temperature mechanics.

To confirm that the changes in modulus are related to progressive loss of crystallinity with increasing temperature, WAXS and FTIR were used to quantify crystallinity with increasing temperature.

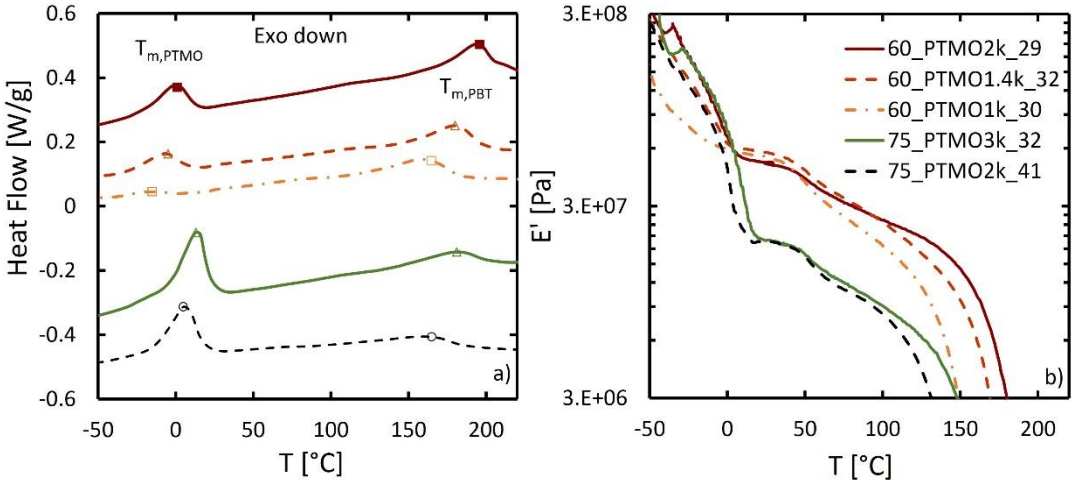

Figure 5 a) DSC thermographs from -50°C to 220°C (2nd heating). Symbol indicate the respective peak maxima. Cooling curves are shown in supplementary material Figure S2. Data are vertically shifted. b) Storage modulus obtained from DMTA. Loss modulus and tanδ related to the same set of samples are shown in supplementary material Figure S3.

The results from X-ray and FTIR analysis shown in Figure 6 corroborate the results obtained from DSC and DMTA and yield a consistent picture with the results from the Flory model. At RT, the crystallinity index calculated strongly decreases with HBwt% and slightly decreases with decreasing SB length. Upon increasing temperature, the decrease in crystallinity is slightly more pronounced for the samples with shorter SB length, as expected from samples with a HB length distribution, and hence melting temperatures distributions, shifted to lower values. These results are consistent with expectation from modeling as indicated by similarities in shape between Figure 6 and Figure 4

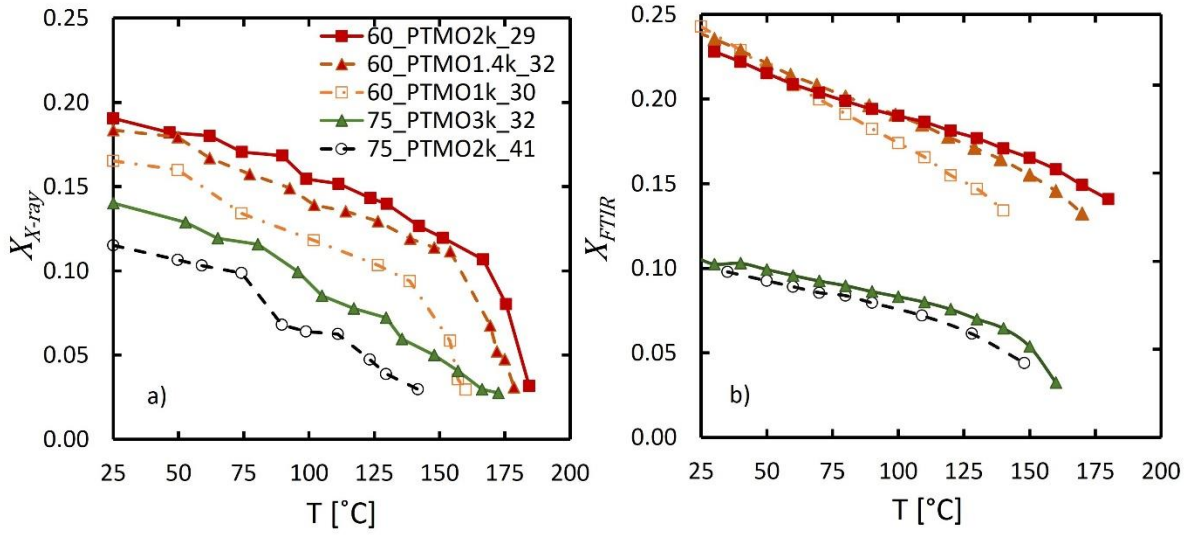

Figure 6 Crystallinity index calculated from WAXS a) and from FT-IR b).

It is worth mentioning that the results from X-ray, FTIR, DSC and DMTA reflect the state of the materials morphology in the undeformed state. The loss of connectivity that occurs during stretching due to HB pull-out will also be influenced by the HB length. While the current analysis focuses on the undeformed state of the material, short HBs in the crystalline forms are likely less resistant to pull-out during stretching than long ones.

In the following section, we discuss the nonlinear properties at high strains of these materials, by means of tensile tests performed at different temperatures.

Quantifying high strain behavior and connectivity: *Tensile and cyclic tests*

Figure 7 shows the tensile curves for RT (a) and 100°C (b). Figure 8 shows the failure strains Vs temperature obtained from tensile tests at different temperatures. At fixed temperature and composition, the curves show a similar tensile behavior up to the yield point, since this region mainly depends on volume fraction of crystals [2]. The high-strain mechanical properties at temperatures lower than ~50 ˚C are strongly influenced by the strain induced crystallization (SIC) of the PTMO SB [32]. The effect of SB length on the SIC has already been investigated via in-situ, under-stretch NMR analysis [18] showing a more pronounced SIC and onset shifted to lower strains for samples with longer SB. Consistent with previous results, we observe an increase in strain hardening with increasing SB length, as a result of more pronounced SIC for those materials. For a pragmatic quantification of the strain hardening, Table SI and SII in the supplementary materials show the stress-strain proportionality constant assuming Neo-Hookean behavior in the strain range 400% < ε < 600%, at RT and 100 °C, respectively. Also note that while no SB crystallinity was observed for the 60_PTMO1k_30 from DSC, it still undergoes SIC [18].

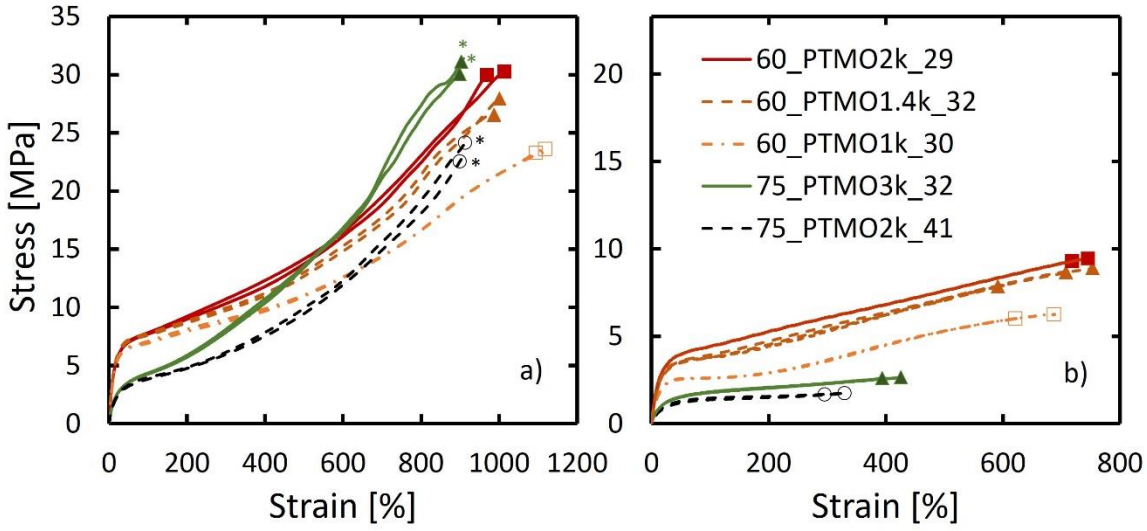

Figure 7 Tensile tests performed at RT (a) and 100 °C (b). Stars indicate that the sample did not reach failure due to reaching of the crosshead displacement limit. Symbols indicate the failure point. Tests performed at 75°C, 125°C, 150°C and 175°C are shown in Figure S4.

At higher temperatures (Figure 7(b)), the yield stress and the overall stress level decrease more for samples with shorter SB. This is consistent with a more pronounced decrease in crystallinity with temperature for samples with shorter SB, supported by the X-ray and FTIR results. The curves show that at higher temperatures the failure strain does not increase with decreasing SB length as could be expected by only considering $< N >$ as an indication for network connectivity. Despite the increase in $< N >$ with decreasing SB length, $< N_{eff} >$ does not increase significantly. Finally, remember the $< N_{eff} >$ is related to the undeformed system. Upon deformation additional HBs are progressively pulled-out from the crystals and an additional effect of SB length on the progressive decrease of connectivity with deformation is expected.

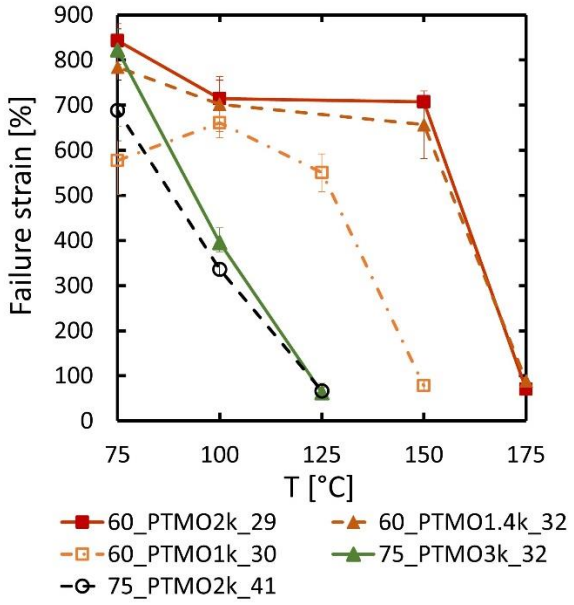

Figure 8 Failure strain versus temperature collected from tensile tests in Figure 7 and supplementary materials. Data at RT are excluded to complications due to influence of SIC.

Cyclic tests are a powerful way to assess the network connectivity in the deformed morphology. The amount of strain recovered after stretching reflects the elasticity of the stretched network and is proportional to the degree of network connectivity.

Figure 9 shows the tensile set (TS) at each step of deformation tested at 100 ˚C for the system with 40% HBwt% calculated from cyclic tests (Figure S5). The curves show a decrease in TS with increasing SB length, highlighting the results at lower applied pre-strain, since the TS is a measure of the recovered strain normalized by the incremental strain at each cycle. Despite the higher degree of crystallinity, often linked to a decrease of the degree of freedom for the molecular chain to move, the sample with longer blocks is more able to recover strain, confirming it to have a better-connected network than the samples with shorter blocks. This shows effectively how in such systems the crystals play the role of physical crosslinks.

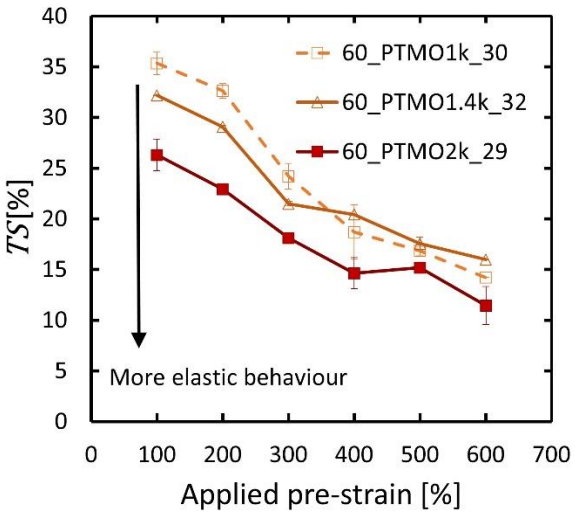

Figure 9 Tensile set (TS) versus the applied pre-strain obtained from cyclic tests performed at 100 °C. The error bars represent the maximum and minimum values for the test repeats.

Conclusions

In this work, we combined morphology and mechanical tests with statistical modeling of block length distribution to bring new insights into the effect of HB length and composition on the high-temperature mechanical properties of soft-TPEs. The results show that in order to improve the temperature mechanical resistance of these systems the *effective numbe*r of associated HB/chain at high temperature must be considered, that is the number of HB/chain that participates in crystals rather than the nominal number of HB/chain. Additionally, we show that the degree of network connectivity, and how it is affected by temperature, is strongly influenced by the HB length and polydispersity, which must be necessarily taken into account when designing high-temperature resistant TPEs. The simple Flory model allows qualitative estimation of how the effective number of HBs per chain decreases with temperature. This approach can be used to select the most suitable material or to design new ones for applications where high-temperature performance is required.

The main results are summarized below:

- HB length polydispersity leads to a broad range of melting temperatures which causes some melting to occur at temperatures much lower than the peak melting temperature of the HB

PBT crystals. Using shorter SBs shifts the average HB length (and T_m) distribution to lower values.

- The number of HB/chain that can crystallize and participate in network connectivity ($<N_{eff}>$) decreases faster with temperature for systems with shorter HBs and is qualitatively described using Flory's theory for random copolymers.
- Connectivity decreases faster at high temperature (due to melting of short HBs) and upon stretching (due to stress-activated pull-out of HB) leading materials with shorter blocks have lower failure strains and overall stresses.
- The ability to recover strain at high temperatures decreases with decreasing HB length, highlighting the crosslinking function of crystallized HBs at high temperatures and deformations.

Supplementary material

See supplementary material for additional details on the FTIR, DSC, DMTA, and tensile tests, as well as further details on the statistical modeling and on the Neo-Hookean analysis of the stress-strain curves.

Acknowledgement

This work was financially supported by funding from the H2020 Program (MARIE SKŁODOWSKA-CURIE ACTIONS) of the European Commission's Innovative Training Networks (H2020-MSCA-ITN-2017) under DoDyNet REA Grant Agreement N°0.765811. The authors thankfully acknowledge Louis Pitet, Olga Goor and the polyester lab in DSM for the synthesis of the model systems, Jildert Overdijk, Anouk van Graven, Junyu Li, and Carole-Ann Charles for the support with the FTIR, DMTA, X-ray, and tensile tests, respectively.

References

[1] Fakirov, S., Handbook of condensation thermoplastic elastomers (Wiley-VCH, Weinheim, 2005).

[2] Nébouy, M., A. De Almeida, S. Brottet, G. P. Baeza, "Process-oriented structure tuning of PBT/PTHF thermoplastic elastomers," Macromolecules **51**, 6291-6302 (2018).

[3] Stevenson, J. C., S. L. Cooper, "Microstructure and property changes accompanying hard-segment crystallization in block copoly (ether-ester) elastomers," Macromolecules **21**, 1309-1316 (1988).

[4] Gabriëlse, W., M. Soliman, K. Dijkstra, "Microstructure and phase behavior of block copoly (ether ester) thermoplastic elastomers," Macromolecules **34**, 1685-1693 (2001).

[5] Litvinov, V. M., M. Bertmer, L. Gasper, D. E. Demco, B. Blümich, "Phase composition of block copoly (ether ester) thermoplastic elastomers studied by solid-state NMR techniques," Macromolecules **36**, 7598-7606 (2003).

[6] De Almeida, A., M. Nébouy, G. P. Baeza, “Bimodal crystallization kinetics of PBT/PTHF segmented block copolymers: Impact of the chain rigidity,” Macromolecules **52**, 1227-1240 (2019).

[7] Smith, T. L., “Tensile strength of polyurethane and other elastomeric block copolymers,” J. Polym. Sci. Part B Polym. Phys. **12**, 1825-1848 (1974).

[8] Gaymans, R. J., “Segmented copolymers with monodisperse crystallizable hard segments: Novel semi-crystalline materials,” Prog. Polym. Sci. **36**, 713-748 (2011).

[9] Konyukhova, E. V., V. M. Neverov, Y. K. Godovsky, S. N. Chvalun, M. Soliman, “Deformation of Polyether-Polyester Thermoelastoplastics: Mechanothermal and Structural Characterisation,” Macromol. Mater. Eng. **287**, 250-265 (2002).

[10] Gorce, J. -N., J. W. Hellgeth, T. C. Ward, “Mechanical hysteresis of a polyether polyurethane thermoplastic elastomer,” Polym. Eng. Sci. **33**, 1170-1176 (1993).

[11] Biemond, G. J. E., J. Feijen, R. J. Gaymans, “Tensile properties of segmented block copolymers with monodisperse hard segments,” J. Mater. Sci. **43**, 3689-3696 (2008).

[12] Aime, S., N. D. Eisenmenger, T. A. P. Engels, “A model for failure in thermoplastic elastomers based on Eyring kinetics and network connectivity,” J. Rheol. **61**, 1329-1342 (2017).

[13] Auriemma, F., C. De Rosa, M. Scoti, R. Di Girolamo, A. Malafronte, M. Christian D’Alterio, L. Boggioni, S. Losio, A. Caterina Boccia, and I. Tritto, “Structure and mechanical properties of ethylene/1-octene multiblock copolymers from chain shuttling technology,” Macromolecules **52**, 2669−2680 (2019).

[14] Sbrescia, S., J. Ju, T. Engels, E. Van Ruymbeke, M. Seitz, “Morphological origins of temperature and rate dependent mechanical properties of model soft thermoplastic elastomers,” J. Polym Sci. **59**, 477– 493, (2021).

[15] Eyring, H., “Viscosity, plasticity, and diffusion as examples of absolute reaction rates,” J. Chem. Phys. **4**, 283-291 (1936).

[16] Xie, H., H.Lu, Z. Zhang, X. Li, X. Yang, Y. Tu, “Effect of Block Number and Weight Fraction on the Structure and Properties of Poly(butylene terephthalate)-block-Poly(tetramethylene oxide) Multiblock Copolymers,” Macromolecules **54**, 2703-2710 (2021).

[17] Apostolov, A. A., S. Fakirov, “Effect of the block length on the deformation behavior of polyetheresters as revealed by small-angle X-ray scattering,” J. Macromol. Sci., Part B **31**, 329-355 (1992).

[18] Schmidt, A., W. S. Veeman, V. M. Litvinov, W. Gabriëlse, “NMR investigations of in-situ stretched block copolymers of poly (butylene terephthalate) and poly (tetramethylene oxide),” Macromolecules **31**, 1652-1660 (1998).

[19] Flory, P. J., “Theory of crystallization in copolymers,” Trans. Faraday Soc. **51**, 848-857 (1955).

[20] Zhang, J., R. Deubler, M. Hartlieb, L. Martin, J. Tanaka, E. Patyukova, P. D. Topham, F. H. Schacher, S. Perrier, “Evolution of microphase separation with variations of segments of sequence-controlled multiblock copolymers,” Macromolecules **50**, 7380-7387 (2017).

[21] Nébouy, M., J. Morthomas, C. Fusco, G. P. Baeza, L. Chazeau, “Coarse-Grained Molecular Dynamics Modeling of Segmented Block Copolymers: Impact of the Chain Architecture on Crystallization and Morphology,“ Macromolecules **53**,3847−3860 (2020).

[22] Ryan, A. J., W. Bras, G. R.Mant, G. E. Derbyshire, “A direct method to determine the degree of crystallinity and lamellar thickness of polymers: application to polyethylene,” Polymer **35**, 4537-4544 (1994).

[23] Jang, J., J. Won, “Crystallisation and phase behaviour of poly (butylene terephthalate)/polyarylate blends,” Polymer **39**, 4335-4342 (1998).

[24] Hopfe, I., G. Pompe, K.-J. Eichhorn, L. Häußler, “FTIR spectroscopy of PC/PBT melt blends: influence of crystallite morphology and copolyester content,” J. Mol. Struct. **349**, 443-446 (1995).

[25] He,Y., Y. Inoue, “Novel FTIR method for determining the crystallinity of poly (ε-caprolactone),” Polym. Int. **49**, 623-626 (2000).

[26] Frensdorff, H. K., “Block-frequency distribution of copolymers,” Macromolecules **4**, 369–375 (1971).

[27] Deschamps, A. A., D. W. Grijpma, J. Feijen, “Poly(ethylene oxide)/poly(butylene terephthalate) segmented block copolymers: the effect of copolymer composition on physical properties and degradation behavior,” Polymer **42**, 9335-9345 (2001).

[28] Boussias, C. M., R. H. Peters, R. H. Still, “Copolyester studies. V. Preparation and characterization of tetramethylene terephthalate–poly (tetramethylene oxide) random block copolymers,” J. Appl. Polym. Sci. **25**, 855-867 (1980).

[29] Van Hutten, P. F., R. M. Mangnus, R. J. Gaymans, “Segmented copolymers with polyesteramide units of uniform length: structure analysis,” Polymer **34**, 4193-4202 (1993).

[30] Fakirov, S., A. A. Apostolov, P. Boeseke, H. G. Zachmann, “Structure of segmented poly (ether ester) s as revealed by synchrotron radiation” J. Macromol. Sci., Part B **29**, 379-395 (1990).

[31] Baeza, G. P., “The reinforcement effect in well-defined segmented copolymers: Counting the topological constraints at the mesoscopic scale,” Macromolecules **51**, 1957-1966 (2018).

[32] Zhu, P., X. Dong, and D. Wang, “Strain-induced crystallization of segmented copolymers: deviation from the classic deformation mechanism,” Macromolecules **50**, 3911-3921 (2017).